OPEN ACCESS

UNIVERSITY OF BRISTOL

Peer reviewed version

Link to published version (if available):
10.1021/jacs.9b07047

Link to publication record in Explore Bristol Research
PDF-document

University of Bristol - Explore Bristol Research
General rights

Photochemistry of Benzophenone in Solution: A Tale of Two Different Solvent Environments

Ravi Kumar Venkatraman†* and Andrew J. Orr-Ewing*

School of Chemistry, University of Bristol, Cantock's Close, Bristol BS8 1TS, United Kingdom

Abstract. A long-standing ambition of photochemists is to excite species selectively in a complex liquid solution, and in turn instigate a controlled chemical reaction. Benzophenone (Bzp) has been studied over six decades as a model system for understanding the photophysics and photochemistry of organic chromophores. Herein, we exploit the red-edge excitation effect to demonstrate that by sub-ensemble selective excitation of Bzp molecules, either coordinated or non-coordinated to phenol through hydrogen bonding in a dichloromethane solution, the rate of an H-atom abstraction reaction can be accelerated by a factor of ~40. To this end, we have employed femtosecond time-resolved electronic and vibrational absorption spectroscopy in conjunction with DFT/TD-DFT calculations. The outcomes have implications for deductions drawn from single-excitation-wavelength studies of the photochemistry of similar molecular systems, and especially of charge-transfer chromophores.

Introduction

Solvent plays a pivotal role in a myriad of chemical and biological processes.[1-15] When a solute is dissolved in a solvent, the resulting solution appears homogeneous at the macroscopic scale, but the solution can remain heterogeneous at the microscopic (sub-ensemble or molecular) scale. This heterogeneity is reflected in solution phase spectroscopy as inhomogeneously broadened spectral peaks. The shifts in spectroscopic transition frequencies manifesting as inhomogeneous line broadening are a consequence of different, and rapidly fluctuating, solvation structures around a solute in a solution.[16] For example, in protic solvents a solute can have distinct solvation states corresponding to hydrogen and non-hydrogen bonded environments.[17] In liquid solutions at ambient temperature, exchange between these different solvent environments can occur on sub-picosecond (sub-ps) to a few picoseconds (ps) timescales, and can be tracked in real time using two-dimensional infrared (2DIR) spectroscopy with sub-ps time resolution.[18-31] Numerous experimental and theoretical investigations have sought to understand the solvation structures around solutes, and their influence on the solute's various physical, chemical and biological properties.[17, 32-43] However, if a sub-ensemble in a solution can be selectively induced to undergo a chemical reaction, the outcome might differ from the ensemble-average outcome expected for a bulk solution. Irradiation with light of carefully chosen wavelength can selectively instigate environment specific chemical reactions, even in a complex heterogeneous medium such as a liquid solution.

We recently demonstrated the sub-ensemble selective photophysics of benzophenone (Bzp) in methanol solution by exploiting the red-edge excitation effect (REEE).[44,45] Absorption of UV either in the long-wavelength region or near the maximum of a π* ← n absorption band of Bzp in methanol solution selectively excites Bzp molecules with their carbonyl group non-coordinated or predominantly coordinated to a methanol solvent molecule by hydrogen bonding, respectively. Furthermore, we observed that the intersystem crossing (ISC) rates of Bzp for these two distinct non-hydrogen bonded and hydrogen bonded (HB) sub-ensembles were altered by approximately an order of magnitude.

The selective photoexcitation of a sub-group of species in a heterogeneous ensemble remains both of fundamental interest and technological importance.[46-51] Herein, we show how selective photoexcitation of molecules in a specific solvation environment can accelerate a bimolecular photochemical reaction by a factor of ~ 40. Our investigations used femtosecond (fs) time-resolved electronic and vibrational absorption spectroscopy measurements (TEAS and TVAS) of supramolecular complexes of Bzp and phenol dissolved in dichloromethane (DCM), with interpretation of the experimental measurements supported by DFT/TD-DFT computations.

Bzp is a model system for the study of the photochemistry of aromatic ketones. It has been subjected to numerous experimental and theoretical investigations because of the importance of Bzp derivatives in technological and biological applications, including photocatalysis, design of compounds for sunscreen formulation, and DNA photosensitization.[52-56] Bzp is known to have a high ISC quantum yield following UV excitation, but until recently the mechanism of population of the lowest triplet excited state (T$_1$) after photoexciting to its S$_1$ (nπ*) state remained uncertain.[57] Our recent work, and computational studies by Gonzalez and coworkers, provide a consistent picture of the ISC mechanism.[44,58] These investigations indicate that the dominant pathway involves fast ISC from S$_1$ to T$_2$ (ππ*) as an intermediate state, with the subsequent rate of population of the lowest vibrational levels of T$_1$ controlled by the timescale for dissipation of excess vibrational energy to the solvent bath after internal conversion (IC) from T$_2$. It is well-

established that after photoexcitation, the long-lived triplet-state Bzp can undergo bimolecular H-atom abstraction reactions with H-atom donor co-reactants.[59-67]

To study the influence of solvation-environment selective excitation on H-atom abstraction reaction rates of photoexcited Bzp, we chose phenol as a co-reactant. There are two main reasons for this choice: (i) phenol is a good H-atom donor;[59-67] and (ii) it can form a supramolecular complex with Bzp by hydrogen bonding. In an equilibrium and fluctuating mixture, the Bzp carbonyl $\pi^* \leftarrow n$ transition of either H-bonded Bzp-phenol supramolecular complexes or non-H-bonded Bzp molecules can be selectively excited. We can therefore study the influence of transient H-bonding interactions on the excited state H-atom abstraction reaction

rate. The participation of an intermediate T_2 state in the mechanism of population of the T_1 state adds an additional possible pathway for H-atom abstraction in the photoexcited Bzp-phenol supramolecular complex. Therefore, a further objective of this study is to understand the mechanistic pathways for H-atom abstraction reactions of photoexcited Bzp coordinated to phenol. Furthermore, this study informs our understanding of the broader dependence of excited state dynamics on the excitation wavelength in similar molecular systems. It shows that care must be taken in drawing conclusions about photophysical, photochemical or photobiological properties of organic chromophores in solution, or in biological media on the basis of experiments conducted at a single excitation wavelength.
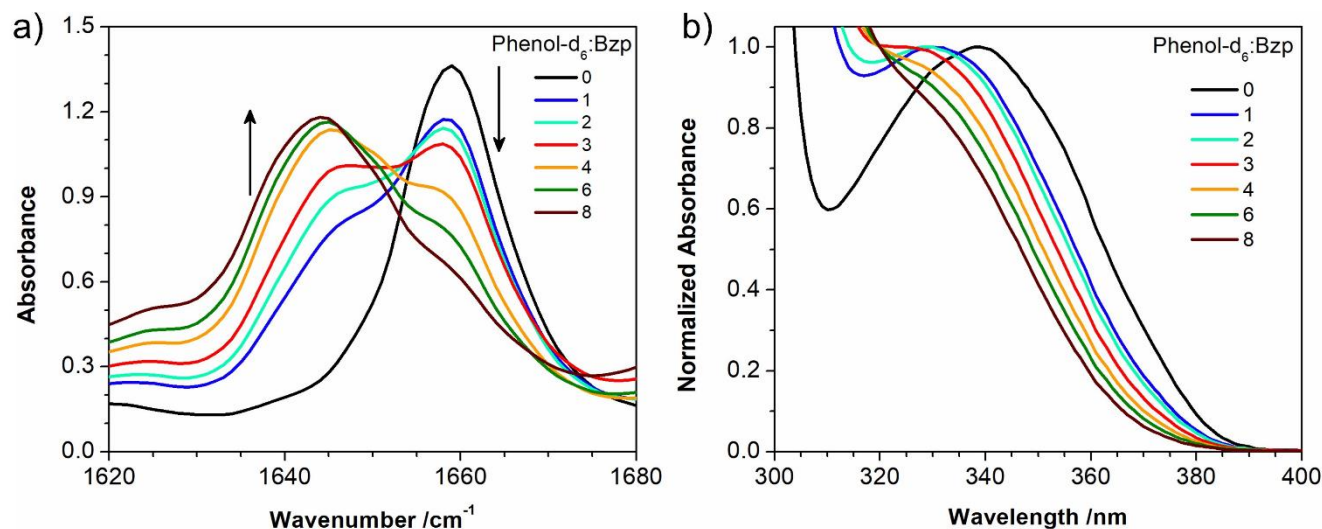

Figure 1. IR and UV absorption spectra of benzophenone / phenol solutions in dichloromethane. a) Steady-state FTIR spectra obtained in the carbonyl stretch wavenumber region. The insets depict the ratios of phenol to Bzp in the mixed solutions. With increasing amounts of phenol, a new peak appears to the low-wavenumber side of the band observed for Bzp in DCM in the absence of phenol, and the arrows indicate the directions of change of the corresponding peak intensities. b) Steady state UV-vis absorption spectra of the $\pi^* \leftarrow n$ transition of Bzp with increasing ratios of phenol in DCM solution. The inset again depicts the ratio of phenol to Bzp.

Results and Discussion

UV-vis and FTIR spectra of Bzp-phenol Supramolecular Complexes. To evaluate the scope for solvation-environment selective excitation of Bzp-phenol supramolecular complexes in dichloromethane solution, steady state UV-vis and FTIR spectroscopic measurements were made for DCM solutions containing different ratios of Bzp and phenol. Phenol-d_6 (written hereafter as phenol for brevity) was used in all the steady-state and time-resolved experiments to ensure an IR-transparent window in the 1400 to 1600 cm^{-1} region for TVAS experiments. The resulting FTIR spectra in the carbonyl stretching frequency region of Bzp are shown in Figure 1a. With increasing amounts of phenol, a new peak appears to lower wavenumber than the Bzp carbonyl stretching peak observed without added phenol. This systematic change in the spectrum indicates that the Bzp molecules exist as sub-populations which are either hydrogen-bonded or non-hydrogen bonded to phenol in DCM, but the absence of an isosbestic point suggests more than two components. A multivariate curve resolution analysis of the Bzp-phenol FTIR spectra (see Figure S1 of Supporting Information) resulted in three peaks identified as Bzp carbonyl groups which are: i) free (uncoordinated); ii) hydrogen

bonded to one phenol; and iii) hydrogen-bonded to a phenol which is itself an acceptor of an H-bond from a further phenol molecule, as indicated by molecular dynamics (MD) simulations (see Figures S2, S3 and S4). These three peaks are more clearly resolved in two-dimensional infrared (2DIR) spectra, as shown in Figure 2 (see Figure S5 for 2DIR spectra of Bzp-phenol in a different ratio), which also reveal the few picosecond timescales for exchange dynamics (see Figure S6 and Table S1). The 2DIR and MD simulation methods and results are discussed further in the Supporting Information. In contrast, the $\pi^* \leftarrow n$ absorption band of Bzp observed in the UV-vis spectrum undergoes a shift to shorter wavelength with increasing amounts of phenol, as shown in Figure 1b. In general, $\pi^* \leftarrow n$ absorption bands undergo hypsochromic shifts with increasing solvent polarity, and the extent of the blue shift of the absorption band with increasing phenol concentration is a direct measure of the ratio of sub-populations of H-bonded and non-H-bonded Bzp carbonyl groups. Hence, red-edge excitation in the long-wavelength tail of the $\pi^* \leftarrow n$ absorption band of Bzp-phenol in DCM solution selectively excites free (non-H-bonded) Bzp carbonyl groups, whereas excitation near the peak wavelength of the band (λ_{max}) predominantly photoexcites Bzp carbonyls which are H-bonded to phenol.
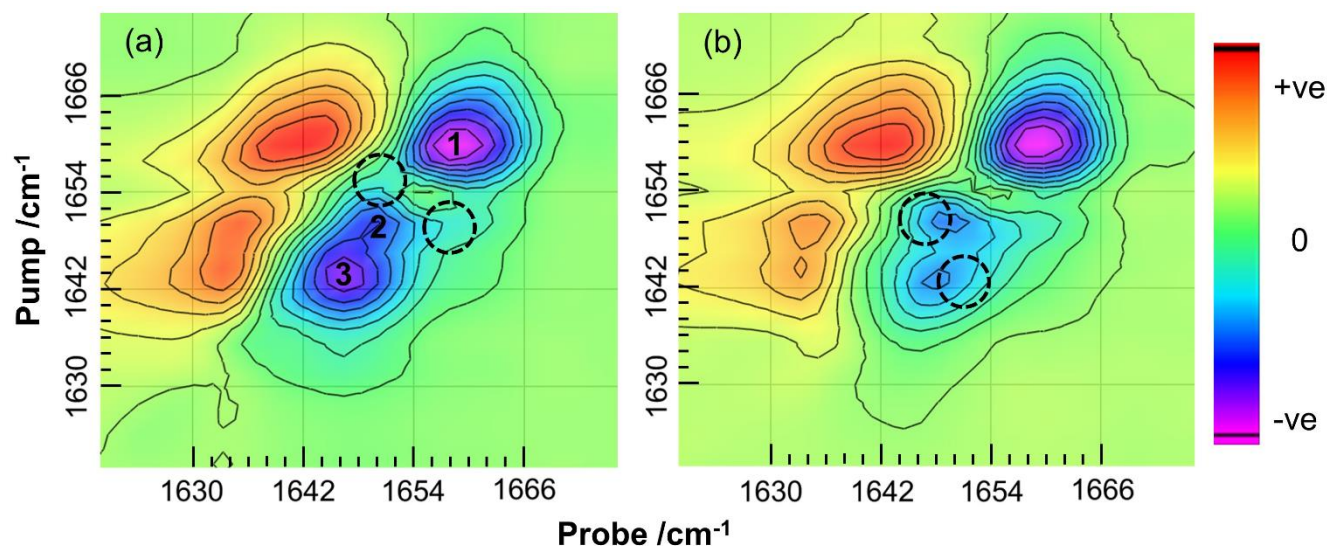
2

Figure 2. 2DIR spectra of 1:3 Bzp-phenol solutions in DCM recorded at waiting times of (a) 100 fs and (b) 1000 fs. The three peaks along the diagonal, designated as peaks 1, 2, 3, are in good agreement with decomposition of the FTIR spectrum (see Figure S1). The right-hand color bar indicates spectral intensities. At different waiting times, cross-peaks between the main diagonal peaks increasingly contribute where indicated by the dashed black circles. These cross-peaks are assigned to exchange dynamics between H-bonded and non-H-bonded structures. The kinetics of the cross-peaks are shown in Figure S6 and their time constants are tabulated in Table S1. See Supporting Information for a detailed discussion.

Femtosecond Time-resolved Electronic and Vibrational Absorption Spectroscopy. The steady-state UV-vis and FTIR absorption spectra reported in Fig. 1 demonstrated the co-existence and scope for selective photoexcitation of Bzp either H-bonded or non-H-bonded to phenol in DCM. To understand the influence of the H-bonding interactions on the photochemistry of Bzp with phenol, we performed ultrafast TEAS and TVAS. To assign the vibrational bands of different species observed in TVAS, we carried out time-dependent density functional theoretical (TD-DFT) calculations. We chose a 1:6 ratio of Bzp to phenol for time-resolved experiments owing to the pronounced selectivity between micro-structures in solution that can be achieved at the excitation wavelengths of 380 nm, 340 nm and 320 nm used in this work (see Figure S7a of Supporting Information). The steady-state UV-vis absorption spectra of 1:6 Bzp-phenol and phenol solutions in DCM are compared in Figure S7b of Supporting Information, and show that the chosen wavelengths exclusively photoexcite the Bzp chromophore.

Figure 3. Time-resolved vibrational absorption spectra of Bzp-phenol (1:6 ratio) in DCM solution obtained following 320 nm

UV excitation. The right-hand key indicates the colour codes for spectra obtained at different time delays (all in ps). The insets show the molecular structures of species proposed to form after photoexcitation.

TEA spectra of Bzp-Phenol H-bonded supramolecular complexes in DCM obtained with 340 nm excitation are shown in Figure S8. The early time spectra are characterized by Bzp S_1 state absorption features, with subsequent population of the T_1 state through the intermediate T_2 state. At longer timescales, absorption bands corresponding to the Bzp ketyl radical appear because of H-atom abstraction from the hydroxyl group of phenol by triplet-state Bzp. Since the excited-state electronic absorption bands are broad, and overlap those of different states or species, it is difficult to discern their kinetics unequivocally. Therefore, we used TVAS to follow more clearly the kinetics of the different species formed by UV photoexcitation.

To identify the different species formed after $\pi^* \leftarrow n$ excitation of Bzp in the presence of phenol in DCM solution, the TVA spectra shown in Figure 3 were recorded with 320 nm excitation. Unlike the TEA spectra, TVA spectra reveal distinct peaks for the Bzp excited states and photoproducts of the H-atom transfer reaction. The prominent peak at 1467 cm^{-1} evident at early times is assigned to the S_1/T_2 state of Bzp, as previously reported.[44] A broad feature at 1515 cm^{-1} grows with a rate matching the decay of the 1467 cm^{-1} peak, and is assigned to the T_1 state of Bzp. The 1515 cm^{-1} band is observed as a long-lived and prominent feature in Bzp/DCM solutions as shown in Figure S9, but in the presence of phenol, the growth in its intensity is inhibited. At longer times, the pronounced peaks centered at 1478 and 1486 cm^{-1} are assigned to Bzp ketyl and phenoxy radical species, respectively. Both bands are absent in Bzp/DCM solutions with no phenol added (see Figure S9). These radical products form through H-atom abstraction from phenol by triplet Bzp. The ground state bleach (GSB) features attributed to Bzp at 1449 and 1572 cm^{-1} change their depths and center
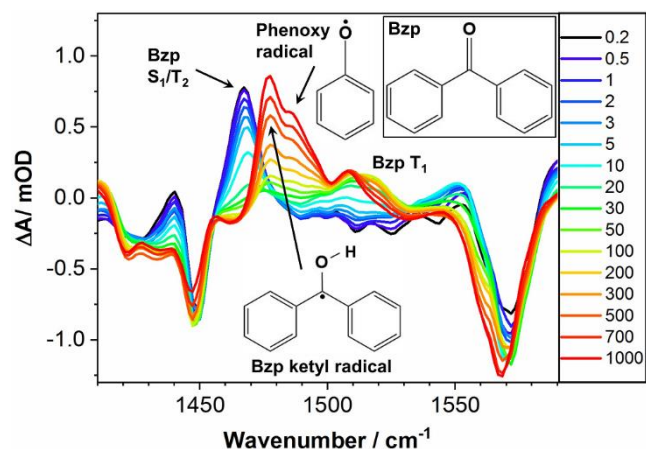
3

Table 1. Vibrational Assignments of Peaks observed in TVA Spectra of Bzp-Phen in DCM solution

electronic states	vibrational frequency /cm^{-1}		vibrational assignments
	exp.	comp. [b]	
S$_1$/T$_2$ [a]	1467	1448	Ring C-H rocking mode
	1555	1566	Ring v(C-C)
T$_1$	1515	1510/1512	Ring v(C-C) + δ(CCH)
Bzp-ketyl radical	1478	1479	Ring C-H rocking mode
	1576	1593	Ring v(C-C)
Phenoxy radical	1486	1500	Ring v(C-C) + δ(CCD)
	1450	1426	v(C-O)

[a]Computation performed for the S$_1$ state only. The assignment to overlapping S$_1$ and T$_2$ bands is discussed in [Ref 44].

[b]Scaled frequencies. See Methods section for a detailed discussion.

positions at longer times, unlike Bzp / DCM solutions without added phenol, suggesting overlapping photoproduct absorptions.

Difference TVA Spectrum and Vibrational Assignments. To assign the peaks observed by TVAS, we simulated the IR spectra of candidate species formed upon photoexcitation (see Methods for a detailed discussion of the computational methods used). The simulation outcomes are shown in Figure 4a. An experimental difference spectrum obtained by subtracting the spectrum recorded at 50 ps from that at 1000 ps is shown in Figure 4b, and is compared with a simulated difference spectrum plotted in Figure 4c and obtained using the component spectra of Fig. 4a.

On this basis, the prominent peaks at 1478 and 1486 cm^{-1} are assigned to the ring C-H rocking mode of the Bzp ketyl radical and the ring C-C and C-H bending of the phenoxy radical, respectively. The photoproduct absorption bands which overlap the Bzp GSB features are also revealed by the analysis presented in Figure 4. Table 1 provides a complete vibrational assignment of the features observed by TVAS, and the atomic displacements of the corresponding normal modes are shown in Figure S10. Further support for our assignments comes from the close agreement of the phenoxy radical peak positions with a previous report of IR bands of photochemically generated phenoxy radicals isolated in an argon matrix.[68]
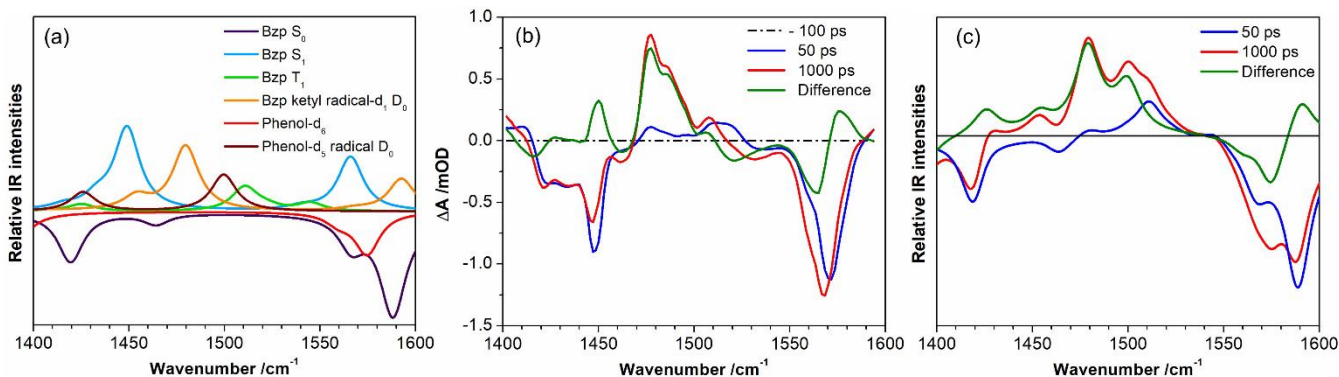

Figure 4. Assignment of bands observed in the TVA spectra of Bzp-Phenol mixtures in DCM solution. (a) Simulated IR spectra of the species proposed to contribute to the TVA spectra in Figure 2. See the Methods section for a summary of the computational methods. (b) The difference TVA spectrum (green solid line) obtained by subtracting the experimental TVA spectrum recorded at 50 ps (blue solid line) from that at 1000 ps (red solid line). (c) The corresponding computed difference spectrum constructed assuming conversion of Bzp(T$_1$) spectral features (present at 50 ps) into those of Bzp and ketyl radicals (at 1000 ps).

A Tale of Two Different Solvent Environments. To revisit the main objective of this study, the TVA spectra obtained at two different UV excitation wavelengths for 1:6 Bzp-phenol solutions in DCM are compared in Figure 5. Pump excitation wavelengths of 340 nm (near λ$_{max}$) and 380 nm (in the long-wavelength tail) were chosen to excite selectively hydrogen-bonded and free carbonyl chromophores of Bzp, respectively. Inspecting the growth of the 1467 cm^{-1} peak (previously assigned to overlapping S$_1$ and T$_2$ state bands of Bzp[44]) at early times reveals subtle differences for the two excitation wavelengths. The integrated peak intensities were fitted to biexponential functions

(Figure 5c and d). At an excitation wavelength of 340 nm, the fits to the integrated intensity of the 1467 cm^{-1} peak returned an early rise component with time constant 1.4 ± 0.8 ps and a later decay with time constant of 8.8 ± 0.9 ps. In contrast, for 380-nm excitation, the initial rise time constant is within the instrument response function (< 0.2 ps), and a later decay with time constant of 10.2 ± 0.3 ps was observed.

These observations are in accord with our recent report on the photoselective excitation of Bzp in methanol solution.[44] A control experiment for Bzp dissolved in DCM without added phenol was carried out at 340 and 380 nm
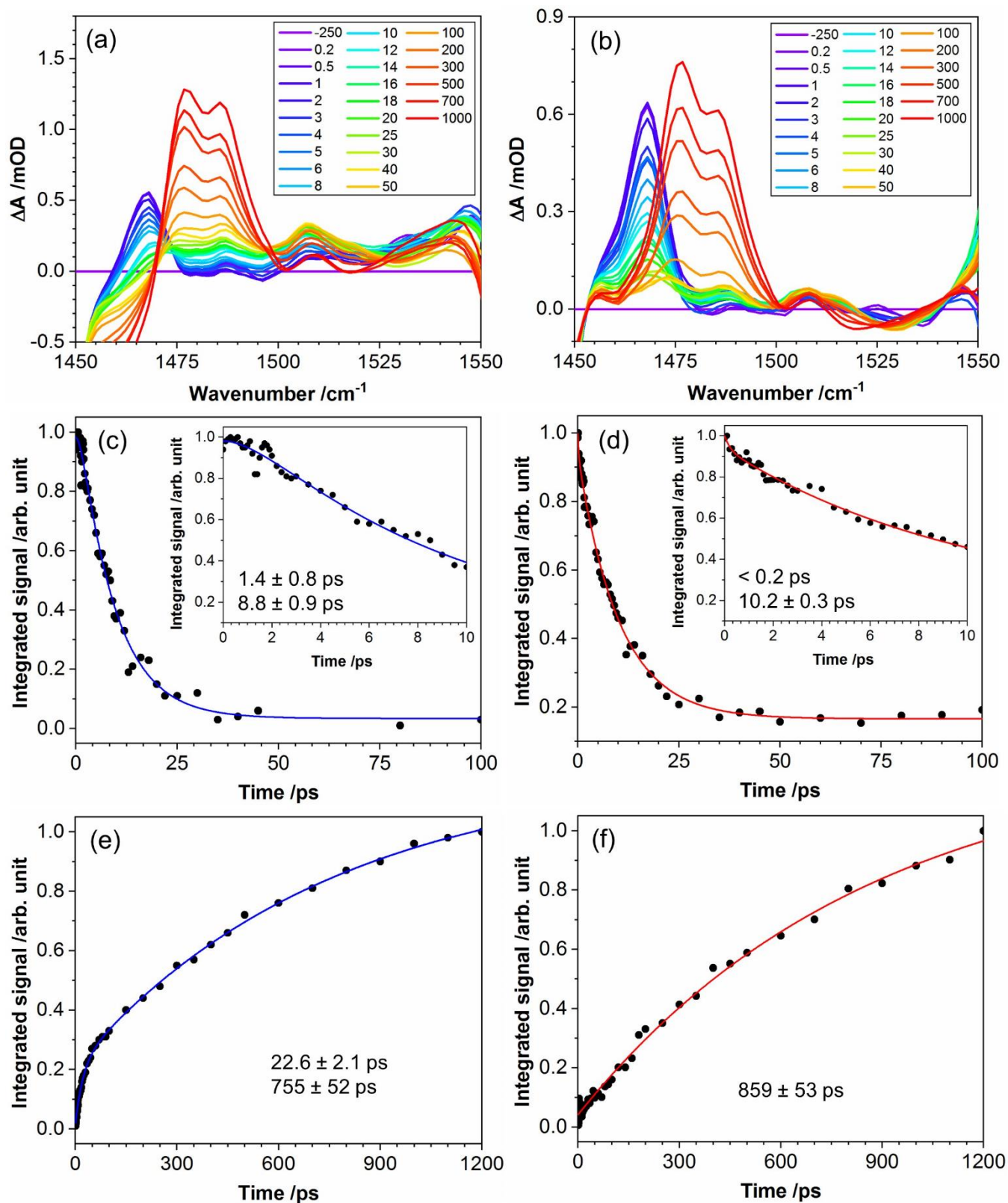
Figure 5. TVA spectra of 1:6 benzophenone: phenol mixtures in dichloromethane obtained at UV excitation wavelengths of (a) 340 nm, and (b) 380 nm. The time dependent integrated band intensities of the 1467 cm^{-1} Bzp (S$_1$/T$_2$) peak are shown at excitation wavelengths of 340 nm in (c) and 380 nm in (d). The insets show expanded views at early time delays. The time dependent integrated band intensities of the product ketyl and phenoxy radical species (1478 and 1486 cm^{-1} peaks) are presented at excitation wavelengths of 340 nm in (e) and 380 nm in (f). The solid lines are bi- or mono-exponential fits to the experimental data (solid circles). To avoid interference of the ground state bleach in the kinetics of the S$_1$/T$_2$ peak (Figure 4a), peak areas were integrated in the 1464 - 1475 cm^{-1} region for 340 nm excitation. In the case of 380 nm excitation, the kinetics obtained from the integrated peak area in the same wavenumber region (not shown) were identical to those obtained by full peak area integration (Figure 4d). The latter method is used for kinetic analysis in this study since the signal obtained with 380 nm is weak relative to 340 nm excitation.

5

excitation wavelengths, and the results presented in Figure S11 show no excitation wavelength dependence. Inspecting the molecular orbitals of $\pi^* \leftarrow n$ and $\pi^* \leftarrow \pi$ electronic transitions and their corresponding electron density difference (see Figure S12), it is evident that hydrogen bonding between Bzp and phenol is weakened by the $S_0 \rightarrow S_1$ excitation, strengthened by the $S_1 \rightarrow T_2$ ISC, and again weakened by the $T_2 \rightarrow T_1$ IC. The hydrogen bonding destabilizes the S_1 ($n\pi^*$) state, but it stabilizes the T_2 ($\pi\pi^*$) state in the Franck-Condon region, thereby lifting the degeneracy of the S_1 and T_2 states and slowing down the ultrafast ISC. Fluctuations in the Bzp-phenol interactions that break intermolecular hydrogen bonds will therefore facilitate the ISC, and these molecular reorganizations act as a kinetic bottleneck.[44] Focusing on the H-atom abstraction reaction between triplet Bzp and phenol, the time evolutions of the 1478 and 1486 cm^{-1} peaks assigned to the Bzp ketyl and phenoxy radicals, respectively, reveal the reaction rate (see Figure 4e and f). At an excitation wavelength of 340 nm, the integrated peak intensities of the radicals grow with bi-exponential time constants of 22.6 ± 2.1 ps and 755 ± 52 ps. In contrast, radical formation following photoexcitation at 380 nm is accounted for by a mono-exponential function with a time constant of 859 ± 53 ps. The time constants obtained are summarized in Table 2.

Table 2. Time Constants Derived from TVAS Measurements for Bzp and Phenol Solutions in DCM for Two Excitation Wavelengths

excitation wavelength (nm)	electronic state/ radicals	time constants (ps)		amplitudes	
		τ_1	τ_2	a_1	a_2
340	Bzp S_1/T_2 [a]	1.4 ± 0.8	8.8 ± 0.9	-0.17 ± 0.08	1.1 ± 0.1
	Bzp ketyl and phenoxy radicals	22.6 ± 2.1	755 ± 52	-0.19 ± 0.01	-1.0 ± 0.1
380	Bzp S_1/T_2 [a]	< 0.2	10.2 ± 0.3	0.06 ± 0.02	0.8 ± 0.1
	Bzp ketyl and phenoxy radicals	-	859 ± 53	-	-1.2 ± 0.1

(a) Time constants are derived from the 1467 cm^{-1} feature in TVA spectra, previously assigned to overlapping absorption bands of the S_1 and T_2 states [Ref. 44].

At both excitation wavelengths, the longer-time radical formation can be ascribed to diffusional bimolecular reaction between Bzp(T_1) (the only long-lived photoexcited state) and phenol. The faster component of radical formation (hereafter referred to as being in the static limit) was observed solely for 340 nm excitation, i.e. for predominantly photoselective excitation of Bzp hydrogen-bonded to phenol, with perhaps a minor contribution from the higher vibronic excitation of free carbonyl Bzp. This prompt reaction exceeds the rate of the diffusional component because the ground-state supramolecular H-bonded complexes are preconfigured for photochemical reaction. These assignments of the fast and slow kinetic components are supported by repeat measurements made for a DCM solution with a lower (1:3) ratio of Bzp:Phenol. Data for the growth of the ketyl and phenoxy radical bands are shown in Figure S13. At an excitation wavelength of 330 nm (chosen such that the amplitude of the static component is similar to that for the 1:6 ratio measurements), the time-constant for the fast component is unchanged (18.9 ± 1.7 ps) whereas the time constant for the slower component increases to ~1200 ps, consistent with diffusive reaction. Only the 1200-ps time constant is observed for an excitation wavelength of 380 nm.

The observed time-dependent first-order rate coefficient $k(t)$ can be expressed as:

$$k(t) = \alpha_\lambda(t)k_1 + \big(1 - \alpha_\lambda(t)\big)k_2[Phenol] \qquad (1)$$

where $k_1 = 1/\tau_1$ is the intrinsic first-order reaction rate constant for H-atom transfer in a reactive Bzp-Phenol complex, and k_2 is the bimolecular rate coefficient for diffusional reaction, such that $1/\tau_2 = k_2[Phenol]$. The parameter $\alpha_\lambda(t)$ is the proportion of complexes pre-configured for reaction following the UV photoexcitation, and decreases rapidly with time as these complexes react. Its initial value depends on the choice of excitation wavelength (λ = 380 nm or 340 nm) in our experiments. The static component observed only for the 340-nm excitation can be attributed to the intrinsic rate constant for the H-atom abstraction reaction.

Reaction within a complex will, like the diffusive component, involve Bzp(T_1). However, the T_2 state, or vibrationally excited T_1-state molecules, which are intermediates in the ISC pathway and survive for a few ps, may also contribute significantly to H-atom transfer and radical formation in the static limit case. To unravel these various possible contributions to reaction, we followed the kinetics of the T_1 state as shown in Figure S14. The amplitudes of the contributing time components of the T_1 state population kinetics were derived by successfully fitting time-dependent T_1 band intensities to exponential functions with time constants constrained to the values obtained from the kinetic analysis of the S_1/T_2, Bzp ketyl and phenoxy radical band intensities (see Table 2). The outcomes of this analysis are summarized in Table S2. The ~12 ps time constant for growth of T_1 population for Bzp in DCM (see Figure S9) is essentially unchanged by addition of phenol ($\tau \sim 10$ ps), and the faster component of T_1 decay following Bzp-phenol complex photoexcitation ($\tau \sim 22$ ps) and attributed to the H-atom transfer reaction is a factor of two slower than this T_1 growth. These observations suggest that at both excitation wavelengths, the reaction mostly happens from the T_1 state after vibrational cooling, with little or no contribution from reaction in the T_2 state or from internally hot T_1 state Bzp. Furthermore, the amplitude ratios obtained are in good agreement with those derived from analysis of the S_1/T_2 and radical band intensities, with opposite signs of the

individual amplitudes in accord with expectations for reaction through the vibrationally equilibrated T_1 state. The H-atom abstraction reaction in the static limit might either happen within Bzp-phenol hydrogen bonded complexes, or between Bzp(T_1) and a phenol molecule in the first solvation shell. One way the latter configuration arises is from ps-timescale dissociation of Bzp-phenol complexes, in which case it can be considered a geminate process. To investigate these possibilities, we followed the rate of exchange between non-hydrogen and hydrogen bonded environments of Bzp with phenol in DCM using 2DIR spectroscopy. These experimental measurements probe the exchange dynamics for Bzp in its ground electronic state. The 2DIR results, which are summarized in the Supporting Information (Figure 2 in the main text, Figures S5, S6 and Table S1), revealed that the exchange between H-bonded and non-H-bonded carbonyl forms of Bzp occurs on timescales from sub-ps to a few ps. The weakening of hydrogen bonds within Bzp-phenol complexes because of IC from the T_2 to the T_1 state was discussed above. Comparing these two deductions, and the known ultrafast timescales for S_1 to T_2 ISC and T_2 to hot T_1 IC, with the observed ~23 ps growth of photoproducts, we propose that H atom abstraction in the static limit case occurs between geminate Bzp and phenol pairs lying within the first solvation shell following dissociation of photoexcited Bzp-phenol complexes. A lower limit of ~16% (see Table 2) was obtained for the H-atom abstraction reactions that happen by these geminate processes following excitation of Bzp-phenol hydrogen-bonded complexes. Assuming that the excitation of Bzp molecules that are not hydrogen bonded to phenol is a small fraction, we further propose that the equilibrium between H-bonded and geminate Bzp (T_1)-phenol pairs favours the latter structures for Bzp(T_1), in contrast to the preference for H-bonded pairs for ground-state Bzp(S_0).

Conclusion. We report the photoselective excitation of sub-ensemble populations of Bzp coordinated or non-coordinated to phenol through hydrogen bonding in DCM solution, and the influence of the H-bonding on the photochemistry, using femtosecond time-resolved absorption spectroscopy. Solvatochromic shifts observed for Bzp and phenol in DCM solutions in UV-vis and FTIR spectroscopy are tell-tale signs for sub-ensemble excitations. TEA and TVA spectra of Bzp and phenol in DCM solution after photoexcitation clearly indicate H-atom abstraction reaction between triplet excited-state Bzp and phenol. Different species observed in TVA spectra are corroborated by DFT/TD-DFT calculations of vibrational band frequencies. With 380-nm excitation. the H-atom abstraction follows diffusive reaction kinetics. In contrast, 340-nm excitation results in H-atom abstraction reactions with rates indicative of both static and diffusive mechanisms. Analysis of the kinetics of the Bzp(T_1) state indicates that the H-atom abstraction reaction happens from this state for both static and diffusive pathways. Inspection of the computed molecular orbitals of Bzp in different electronic states shows that the hydrogen bond with phenol is weakened in the T_1 state compared to S_0 or T_2. Therefore, we propose that accelerated H-atom transfer from phenol to Bzp(T_1) in the static limit following photoexcitation of H-bonded Bzp(S_0)-phenol complexes occurs from vibrationally thermalized Bzp (T_1) molecules, and that the weaker Bzp(T_1)-phenol H-bonds break before the H-atom transfer occurs.

ASSOCIATED CONTENT

Supporting Information. "This material is available free of charge via the Internet at http://pubs.acs.org." Experimental and computational methods, Multivariate analyzed FTIR spectra of Bzp-phenol in DCM solution, Histogram plot of hydrogen and non-hydrogen bonded populations of Bzp carbonyl (from MD simulations), radial distribution functions of the Bzp carbonyl oxygen atom and the protic hydrogen and oxygen atoms of phenol (from MD simulations), representative solvation structures of Bzp (from MD Simulations), 2DIR spectra of Bzp-phenol in DCM solution at different ratios, Kinetic plots for the cross-peaks of 2DIR spectra of Bzp-phenol (1:3) in DCM solution and their time constants, Steady state UV-vis spectra of Bzp, phenol and their mixtures, TEA spectra of a Bzp-phenol mixture in DCM solution, TVA spectra of a Bzp/DCM solution at two excitation wavelengths, Normal mode vibrations of Bzp, Bzp ketyl and phenoxy radicals, Frontier molecular orbitals of Bzp and their corresponding electron density differences, Kinetic analysis of TVA spectra of a Bzp/DCM solution at two excitation wavelengths, Kinetic analysis of the T_1 state of Bzp-phenol in DCM solution at two excitation wavelengths, and Amplitudes derived for the T_1 kinetics of Bzp and phenol solutions in DCM at two excitation wavelengths.

AUTHOR INFORMATION

Corresponding Authors

*ravi.venkatraman@austin.utexas.edu
*a.orr-ewing@bristol.ac.uk

Present Address

†Department of Chemistry, University of Texas at Austin, Austin, Texas 78712, United States

ABBREVIATIONS

REEE, Red-edge Excitation Effect; TEAS, Time-resolved Electronic Absorption Spectroscopy; TVAS, Time-resolved Vibrational Absorption Spectroscopy; ISC, Intersystem Crossing.

REFERENCES

(1) Reichardt, C. Introduction. In *Solvents and Solvent Effects in Organic Chemistry*; John Wiley & Sons, Ltd, 2010; pp 1–5.

(2) Barbara, P. F.; Walker, G. C.; Smith, T. P. Vibrational Modes and the Dynamic Solvent Effect in Electron and Proton Transfer. *Science* **1992**, *256*, 975–981.

(3)   Bellissent-Funel, M. C.; Hassanali, A.; Havenith, M.; Henchman, R.; Pohl, P.; Sterpone, F.; Van Der Spoel, D.; Xu, Y.; Garcia, A. E. Water Determines the Structure and Dynamics of Proteins. *Chem. Rev.* **2016**, *116*, 7673–7697.

(4)   Cainelli, G.; Galletti, P.; Giacomini, D. Solvent Effects on Stereoselectivity: More than Just an Environment. *Chem. Soc. Rev.* **2009**, *38*, 990–1001.

(5)   Elles, C. G.; Crim, F. F. Connecting Chemical Dynamics in Gases and Liquids. *Annu. Rev. Phys. Chem.* **2006**, *57*, 273–302.

(6)   Halpern, J.; Orgel, L. E. Electron-Transfer Reactions. *Discuss. Faraday Soc.* **1960**, *29*, 7–20.

(7)   Havenith, M. Solvation Science: A New Interdisciplinary Field. *Angew. Chemie - Int. Ed.* **2016**, *55*, 1218–1219.

(8)   Lin, Y.-H.; Yin, C.; Lin, W.-H.; Li, Y.-L.; Takahashi, K.; Lin, J. J.-M. Criegee Intermediate Reaction with Alcohol Is Enhanced by a Single Water Molecule. *J. Phys. Chem. Lett.* **2018**, *9*, 7040–7044.

(9)   Balakrishnan, G.; Sahoo, S. K.; Chowdhury B. K.; Umapathy S. Understanding solvent effects on structure and reactivity of organic intermediates: a Raman study. *Faraday Discuss.* **2010**, *145*, 443–466.

(10)   Morgenstern, K.; Marx, D.; Havenith, M.; Muhler, M. Editorial of the PCCP Themed Issue on "Solvation Science." *Phys. Chem. Chem. Phys.* **2015**, *17*, 8295–8296.

(11)   Orr-Ewing, A. J. Taking the Plunge: Chemical Reaction Dynamics in Liquids. *Chem. Soc. Rev.* **2017**, *46*, 7597–7614.

(12)   Papoian, G. A.; Ulander, J.; Eastwood, M. P.; Luthey-Schulten, Z.; Wolynes, P. G. From The Cover: Water in Protein Structure Prediction. *Proc. Natl. Acad. Sci.* **2004**, *101*, 3352–3357.

(13)   Struebing, H.; Ganase, Z.; Karamertzanis, P. G.; Siougkrou, E.; Haycock, P.; Piccione, P. M.; Armstrong, A.; Galindo, A.; Adjiman, C. S. Computer-Aided Molecular Design of Solvents for Accelerated Reaction Kinetics. *Nat. Chem.* **2013**, *5*, 952–957.

(14)   Sun, Q.; Wang, S.; Aguila, B.; Meng, X.; Ma, S.; Xiao, F. S. Creating Solvation Environments in Heterogeneous Catalysts for Efficient Biomass Conversion. *Nat. Commun.* **2018**, *9*, 3236.

(15)   Widmer, D. R.; Schwartz, B. J. Solvents Can Control Solute Molecular Identity. *Nat. Chem.* **2018**, *10*, 910–916.

(16)   Sevian, H. M.; Skinner, J. L. A Molecular Theory of Inhomogeneous Broadening, Including the Correlation between Different Transitions, in Liquids and Glasses. *Theor. Chim. Acta* **1992**, *82*, 29–46.

(17)   Kumar, V. R.; Verma, C.; Umapathy, S. Molecular Dynamics and Simulations Study on the Vibrational and Electronic Solvatochromism of Benzophenone. *J. Chem. Phys.* **2016**, *144*, 064302.

(18)   Tokmakoff, A. Shining Light on the Rapidly Evolving Structure of Water. *Science.* **2007**, *317*, 54–55.

(19)   Hamm, P.; Zanni, M. *Concepts and Methods of 2D Infrared Spectroscopy*; Cambridge University Press: Cambridge, 2011.

(20)   Tokmakoff, A. Structural Rearrangements in Water Viewed Spectroscopy. *Acc. Chem. Res.* **2009**, *42*, 1239.

(21)   Bakulin, A. A.; Liang, C.; Jansen, T. L. A. C.; Wiersma, D. A.; Bakker, H. J.; Shenichnikov, M. S. P. Hydrophobic Solvation: A 2D IR Spectroscopic Inquest. *Acc. Chem. Res.* **2009**, *42*, 1229–1238.

(22)   Cazade, P. A.; Tran, H.; Bereau, T.; Das, A. K.; Kläsi, F.; Hamm, P.; Meuwly, M. Solvation of Fluoro-Acetonitrile in Water by 2D-IR Spectroscopy: A Combined Experimental-Computational Study. *J. Chem. Phys.* **2015**, *142*, 212415.

(23)   Jones, B. H.; Huber, C. J.; Massari, A. M. Solvation Dynamics of Vaska's Complex by 2D-IR Spectroscopy. *J. Phys. Chem. C* **2011**, *115*, 24813–24822.

(24)   Zheng, J.; Kwak, K.; Fayer, M. D. Ultrafast 2D IR Vibrational Echo Spectroscopy. *Acc. Chem. Res.* **2007**, *40*, 75–83.

(25)   Fayer, M. D. Dynamics of Liquids, Molecules, and Proteins Measured with Ultrafast 2D IR Vibrational Echo Chemical Exchange Spectroscopy. *Annu. Rev. Phys. Chem.* **2009**, *60*, 21–38.

(26)   Kim, Y. S.; Hochstrasser, R. M. Chemical Exchange 2D IR of Hydrogen-Bond Making and Breaking. *Proc. Natl. Acad. Sci.* **2005**, *102*, 11185–11190.

(27)   Dahms, F.; Fingerhut, B. P.; Nibbering, E. T. J.; Pines, E.; Elsaesser, T. Large-Amplitude Transfer Motion of Hydrated Excess Protons Mapped by Ultrafast 2D IR Spectroscopy. *Science.* **2017**, *357*, 491–495.

(28)   Moilanen, D. E.; Wong, D.; Rosenfeld, D. E.; Fenn, E. E.; Fayer, M. D. Ion-Water Hydrogen-Bond Switching Observed with 2D IR Vibrational Echo Chemical Exchange Spectroscopy. *Proc. Natl. Acad. Sci.* **2009**, *106*, 375–380.

(29)   Park, S.; Fayer, M. D. Hydrogen Bond Dynamics in Aqueous NaBr Solutions. *Proc. Natl. Acad. Sci.* **2007**, *104*, 16731–16738.

(30)   Woutersen, S.; Mu, Y.; Stock, G.; Hamm, P. Hydrogen-Bond Lifetime Measured by Time-Resolved 2D-IR Spectroscopy: N-Methylacetamide in Methanol. *Chem. Phys.* **2001**, *266*, 137–147.

(31)   Demirdöven, N.; Khalil, M.; Tokmakoff, A. Correlated Vibrational Dynamics Revealed by Two-Dimensional Infrared Spectroscopy. *Phys. Rev. Lett.* **2002**, *89*, 1–4.

(32)   Bagchi, B. Water Dynamics in the Hydration Layer around Proteins and Micelles. *Chem. Rev.* **2005**, *105*, 3197-3219.

(33)   Davis, J. G.; Gierszal, K. P.; Wang, P.; Ben-Amotz, D. Water Structural Transformation at Molecular Hydrophobic Interfaces. *Nature* **2012**, *491*, 582–585.

(34)   Groot, C. C. M.; Bakker, H. J. Proteins Take up Water before Unfolding. *J. Phys. Chem. Lett.* **2016**, *7*, 1800–1804.

(35)   Hamm, P.; Savolainen, J. Two-Dimensional-Raman-Terahertz Spectroscopy of Water: Theory. *J. Chem. Phys.* **2012**, *136*, 1–6.

(36)   Oh, K. I.; Rajesh, K.; Stanton, J. F.; Baiz, C. R. Quantifying Hydrogen-Bond Populations in Dimethyl Sulfoxide/Water Mixtures. *Angew. Chemie - Int. Ed.* **2017**, *56*, 11375–11379.

(37)   Perera, P. N.; Fega, K. R.; Lawrence, C.; Sundstrom, E. J.; Tomlinson-Phillips, J.; Ben-Amotz, D. Observation of Water Dangling OH Bonds around Dissolved Nonpolar Groups. *Proc. Natl. Acad. Sci. U. S. A.* **2009**, *106*, 12230–12234.

(38)   Ramakrishnan, G.; González-Jiménez, M.; Lapthorn, A. J.; Wynne, K. Spectrum of Slow and Super-Slow (Picosecond to Nanosecond) Water Dynamics around Organic and Biological Solutes. *J. Phys. Chem. Lett.* **2017**, *8*, 2964–2970.

(39)   Schienbein, P.; Schwaab, G.; Forbert, H.; Havenith, M.; Marx, D. Correlations in the Solute-Solvent Dynamics Reach beyond the First Hydration Shell of Ions. *J. Phys. Chem. Lett.* **2017**, *8*, 2373–2380.

(40)   Schwaab, G.; Sebastiani, F.; Havenith, M. Ion Hydration and Ion Pairing as Probed by THz Spectroscopy. *Angew. Chemie, Int. Ed.* **2019**, *58*, 3000-3013.

(41)   Tielrooij, K. J.; Bonn, M.; Bakker, H. J. Cooperativity in Ion Hydration. *Science.* **2010**, *328*, 1006–1009.

(42)   Wu, B.; Maroncelli, M.; Castner, E. W. Photoinduced Bimolecular Electron Transfer in Ionic Liquids. *J. Am. Chem. Soc.* **2017**, *139*, 14568–14585.

(43)   Ben-Amotz, D. Hydration-Shell Vibrational Spectroscopy. *J. Am. Chem. Soc.* **2019**, *141*, 10569-10580.

(44)   Venkatraman, R. K.; Kayal, S.; Barak, A.; Orr-Ewing, A. J.; Umapathy, S. Intermolecular Hydrogen Bonding Controlled Intersystem Crossing Rates of Benzophenone. *J. Phys. Chem. Lett.* **2018**, *9*, 1642–1648.

(45)   Demchenko, A. P. The Red-Edge Effects: 30 Years of Exploration. *Luminescence* **2002**, *17*, 19–42.

(46)   Kern-Michler, D.; Neumann, C.; Mielke, N.; Van Wilderen, L. J. G. W.; Reinfelds, M.; Von Cosel, J.; Santoro, F.; Heckel, A.; Burghardt, I.; Bredenbeck, J. Controlling Photochemistry via Isotopomers and IR Pre-Excitation. *J. Am. Chem. Soc.* **2018**, *140*, 926–931.

(47)   Letrun, R.; Vauthey, E. Excitation Wavelength Dependence of the Dynamics of Bimolecular Photoinduced Electron Transfer Reactions. *J. Phys. Chem. Lett.* **2014**, *5*, 1685–1690.

(48)   Samanta, A. Solvation Dynamics in Ionic Liquids: What We Have Learned from the Dynamic Fluorescence Stokes Shift Studies. *J. Phys. Chem. Lett.* **2010**, *1*, 1557–1562.

(49)   Tang, L.; Liu, W.; Wang, Y.; Zhu, L.; Han, F.; Fang, C. Ultrafast Structural Evolution and Chromophore Inhomogeneity inside a Green-Fluorescent-Protein-Based Ca2+Biosensor. *J. Phys. Chem. Lett.* **2016**, *7*, 1225–1230.

(50)   van Wilderen, L. J. G. W.; Messmer, A. T.; Bredenbeck, J. Mixed IR/Vis Two-Dimensional Spectroscopy: Chemical Exchange beyond the Vibrational Lifetime and Sub-Ensemble Selective Photochemistry. *Angew. Chemie - Int. Ed.* **2014**, *53*, 2667–2672.

(51)   Mishra, P.; Jha, S. K. Slow Motion Protein Dance Visualized Using Red-Edge Excitation Shift of a Buried Fluorophore. *J. Phys. Chem. B* **2019**, *123*, 1256–1264.

(52)   Dormán, G.; Nakamura, H.; Pulsipher, A.; Prestwich, G. D. The Life of Pi Star: Exploring the Exciting and Forbidden Worlds of the Benzophenone Photophore. *Chem. Rev.* **2016**, *116*, 15284–15398.

(53)   Cuquerella, M. C.; Lhiaubet-Vallet, V.; Cadet, J.; Miranda, M. A. Benzophenone Photosensitized DNA Damage. *Acc. Chem. Res.* **2012**, *45*, 1558–1570.

(54)   Rajagopal, S. K.; Sebastian, E.; Bhat, V.; K., N.; Deb, S.; Sasikumar, D.; Hariharan, M. Extending the Scope of the Carbonyl Facilitated Triplet Excited State towards Visible Light Excitation. *Phys. Chem. Chem. Phys.* **2018**, *20*, 19120–19128.

(55)   Zvereva, E.; Segarra-Martí, J.; Marazzi, M.; Brazard, J.; Nenov, A.; Weingart, O.; Léonard, J.; Garavelli, M.; Rivalta, I.; Dumont, E.; et al. The Effect of Solvent Relaxation in the Ultrafast Time-Resolved Spectroscopy of Solvated Benzophenone. Photochem. Photobiol. Sci. 2018, 17, 323–331.

(56)   Marazzi, M.; Wibowo, M.; Gattuso, H.; Dumont, E.; Roca-Sanjuán, D.; Monari, A. Hydrogen Abstraction by Photoexcited Benzophenone: Consequences for DNA Photosensitization. Phys. Chem. Chem. Phys. 2016, 18, 7829–7836.

(57)   McGarry, P. F.; Doubleday, C. E.; Wu, C. H.; Staab, H. A.; Turro, N. J. UV-Vis Absorption Studies of Singlet to Triplet Intersystem Crossing Rates of Aromatic Ketones: Effects of Molecular Geometry. J. Photochem. Photobiol. A Chem. 1994, 77, 109–117.

(58)   Marazzi, M.; Mai, S.; Roca-Sanjuán, D.; Delcey, M. G.; Lindh, R.; González, L.; Monari, A. Benzophenone Ultrafast Triplet Population: Revisiting the Kinetic Model by Surface-Hopping Dynamics. J. Phys. Chem. Lett. 2016, 7, 622–626.

(59)   Das, P. K.; Encinas, M. V.; Scaiano, J. C. Laser Flash Photolysis Study of the Reactions of Carbonyl Triplets with Phenols and Photochemistry of P-Hydroxypropiophenone. J. Am. Chem. Soc. 1981, 103, 4154–4162.

(60)   Leigh, W. J.; Lathioor, E. C.; St. Pierre, M. J. Photoinduced Hydrogen Abstraction from Phenols by Aromatic Ketones. A New Mechanism for Hydrogen Abstraction by Carbonyl n,π* Triplets. J. Am. Chem. Soc. 1996, 118, 12339–12348.

(61)   Litwinienko, G.; Ingold, K. U. Solvent Effects on the Rates and Mechanisms of Reaction of Phenols with Free Radicals. Acc. Chem. Res. 2007, 40, 222–230.

(62)   MacFaul, P. A.; Ingold, K. U.; Lusztyk, J. Kinetic Solvent Effects on Hydrogen Atom Abstraction from Phenol, Aniline, and Diphenylamine. The Importance of Hydrogen Bonding on Their Radical-Trapping (Antioxidant) Activities. J. Org. Chem. 1996, 61, 1316–1321.

(63)   Walling, C.; Gibian, M. J. Hydrogen Abstraction by the Triplet State of Benzophenone [29]. J. Am. Chem. Soc. 1964, 86, 3902–3903.

(64)   Walling, C.; Gibian, M. J. Hydrogen Abstraction Reactions by the Triplet States of Ketones. J. Am. Chem. Soc. 1965, 87, 3361–3364.

(65)   Wagner, P.; Park, B. S. Photoinduced Hydrogen Atom Abstraction Reaction by Carbonyl Compounds. In *Organic Photochemistry*; Padwa, A., Ed.; Marcel Dekker: New York, 1991; pp 227–366.

(66)   N. J. Turro, *Modern Molecular Photochemistry*; University Science Books: Sausalito, 1991; pp 362-413 and references therein.

(67)   N. J. Turro, V. Ramamurthy, and J. C. Scaiano, *Modern Molecular Photochemistry of Organic Molecules*; University Science Books: Sausalito, 2010.

(68)   Spanget-Larsen, J.; Gil, M.; Gorski, A.; Blake, D. M.; Waluk, J.; Radziszewski, J. G. Vibrations of the Phenoxyl Radical. *J. Am. Chem. Soc.* **2001**, *123*, 11253–11261.

Table of content graphics only